



Simple and green synthesis of carbon dots (CDs) from valerian root and application of modified mesoporous boehmite (AlOOH) with CDs as a fluorescence probe for determination of imipramine

Reyhaneh Sobhani¹ · Behzad Rezaei¹ · Marzieh Shahshahanipour¹ · Ali A. Ensafi¹ · Gholamhossein Mohammadnezhad¹

Received: 19 December 2018 / Revised: 18 February 2019 / Accepted: 11 March 2019 / Published online: 15 April 2019
© Springer-Verlag GmbH Germany, part of Springer Nature 2019

Abstract

A novel, sensitive, rapid, and simple fluorescent probe has been developed based on green-synthesized carbon dots (CDs). In this work, CDs have been synthesized from valerian root by hydrothermal method. Transmission electron microscopy (TEM) and dynamic light scattering (DLS) results confirm the formation of CDs with sizes of less than 10 nm. Fluorescence quenching of CDs was due to the aggregation of the negative charges of CDs with the positive charge of imipramine (IMI) and was then used as the signal for determination of IMI. In addition, the cytotoxicity of CDs was determined using the MTT assay. The probe responses under optimum conditions were linear in the range of 1.0–200.0 ng mL⁻¹ with a limit of detection of 0.6 ng mL⁻¹. Afterwards, mesoporous boehmite (MB) was modified with synthesized CDs (CDs/MB). TEM images confirmed MB modification with CDs. In this case, the variations in the fluorescence signal for different concentrations of IMI increased leading to the higher sensitivity for IMI detection. The limit of detection and linear range for determination of IMI with CDs/MB were obtained as 0.2 and 0.5–200.0 ng mL⁻¹, respectively. To evaluate the fluorescent probe, IMI was measured in real samples.

Keywords Green carbon dots · Modified mesoporous boehmite with CDs · Fluorescent probe · Imipramine

Introduction

In the modern world, depression is one of the most important impairments in mental health and the treatment is very important [1, 2]. Imipramine (IMI) is one of the tricyclic antidepressant (TCA) drugs, which are the most common and effective for the treatment of psychiatric disorders, especially depressions [3]. This drug elevates the mood of patients by interfering with the reuptake of norepinephrine or serotonin [4, 5]. Similar to other psychiatric medications, IMI leads to some adverse effects. The common side effects of consuming IMI include low blood pressure, rapid heart rate, dizziness, dry mouth, drowsiness, and overdose, which can result in death [6]. The symptoms of taking too much IMI include uncontrol-

lable body movements, seizure, and coma [7, 8]. Therefore, a fast determination of IMI with high sensitivity and precision is essential. Several analytical methods have been reported for the determination of IMI in human fluids. These methods include high-performance liquid chromatography (HPLC), capillary electrophoresis, thin layer chromatography, electro-analytical methods, and atomic absorption spectrometry [9, 10]. However, many of these methods are limited in terms of their application and equipment. The fluorescent based method was considered because of its high degree of sensitivity and specificity, relative simplicity, fastness, and less expense compared with the other methods for the determination of the low concentrations of the drug [11]. In this work, fluorescence assays have been evaluated based on the aggregation and electron transfer of CDs for the determination of IMI.

Carbon nanomaterials have received a huge amount of research interest, especially for sensing applications. The large surface area of nanoparticles provides a great number of active sites in which target molecules can bind and interact [12].

CDs have recently gained great attention because of their interesting properties such as high solubility, high fluorescent

✉ Behzad Rezaei
rezaei@cc.iut.ac.ir

¹ Department of Chemistry, Isfahan University of Technology, Isfahan 84156–83111, Iran

properties, the surface modification capability, tunable excitation, emission wavelength, and high resistance to photobleaching. Furthermore, biological potentials of CDs enable them for in vivo determination [13]. Emission in the visible region makes CDs applicable in optical tools. Their rather broad absorption spectra enable different sizes of CDs to be excited by only a single source [14]. The synthesis of CDs with high fluorescent emission in the visible range by simple, inexpensive, and green methods has been recently considered. In this work, Valerian root was utilized for the first time as a carbon source to produce new CDs. Valerian is an herbal product used to promote sleep and an anxiolytic for nervous unrest, epilepsy, and spasmolytic effects. Valerian roots affect stress and neuralgia [15]. In this work, the aggregation behavior, in which the changes in light scattering were measured as a response function of the probe, was effective in changing the intensity of fluorescence. The aggregation mechanism can be confirmed by using several techniques such as fluorescence spectroscopy, TEM, and zeta potential measurement. Furthermore, the DLVO (Derjaguin, Landau, Verwey, and Overbeek) theory can be used to justify the experimental results [16]. In the next step, boehmite (AlOOH), one of the most stable mesoporous materials, which is non-toxic and inexpensive and has a high surface area and porosity, is used as a support for CDs [17–19]. Modification of the surface of the mesoporous boehmite (MB) makes it useful in targeting applications. There are many hydroxyl groups on the surface layered structure of MB, which can bind with hydroxyl groups on the CDs [20, 21]. MB modified with CDs shows increased fluorescence intensity due to its high rigidity.

Sensing the response to the changes in the emission intensity of CDs can be connected by electron transfer mechanism, which occurs when an electron relocates from an atom or molecule to another such chemical entity. It is based on the electrostatic adsorption of cationic quencher on the surface of anionic CDs [22].

Materials and methods

Chemicals

All the chemicals were of analytical grade or of the highest available purity and distilled water was used throughout the experiments. Valerian root, as the carbon source, was purchased from a local market. Imipramine hydrochloride ($\geq 99.0\%$) was obtained from Amin Drug Company (Esfahan, Iran). Human liver cancer (HepG2) and cervical cancer (HeLa) cell lines were obtained from Pasteur Institute (Iran, Tehran). Universal buffer solution (0.04 mol L^{-1}) at pH 6.0 was prepared by phosphoric acid (H_3PO_4), boric acid (H_3BO_3), and citric acid (CH_3COOH) (each of them in 0.04 mol L^{-1}) and that titrated to the desired pH with the

appropriate amount of sodium hydroxide NaOH (0.2 mol L^{-1}) [6]. Ethanol ($\text{C}_2\text{H}_5\text{OH}$), iso-propanil, chloride salts of Ni^{2+} , Hg^{2+} , Fe^{2+} , Cu^{2+} , Zn^{2+} , L-cysteine, glutathione (GSH), ammonium acetate, Rhodamine B (RhB), and methyl thiazolyl diphenyltetrazolium bromide (MTT) were purchased from Sigma Aldrich Chemical Co. Acetonitrile (ACN) and methanol HPLC-grade were supplied from Merck (Darmstadt, Germany). Pure water was obtained by OES system (Oklahoma, USA). Aluminum iso-propoxide was synthesized based on a previously published procedure [23].

Apparatus

UV–Vis light absorption spectra were obtained using a Jasco V-570 UV/Vis/NIR spectrophotometer (Tokyo, Japan). Fluorescence spectra were recorded on a Jasco FP-750 spectrofluorometer (Tokyo, Japan). TEM experiments were carried out with a Philips CM30 300 kV TEM (Eindhoven, The Netherlands). Fourier-transform infrared spectra (FTIR) were recorded on a JASCO FTIR (680 plus) spectrophotometer (Tokyo, Japan) to obtain information about the functional groups of CDs. The particle size distribution was determined using a Malvern ZEN3600 DLS instrument (Birmingham, UK). X-ray diffraction (XRD) analyses were carried out with a Bruker D8/Advance X-ray (Washington, USA). Energy dispersive X-ray spectroscopy (EDX) was carried out with a Seron AIS 2300 (Korea). A coring pH meter, model 827 pH Lab (New York, USA) was used to determine the pH of the solution. A Malvern Zetasizer NanoZS, Model ZEN3600 (UK) was used for zeta potential measurements. Chromatographic separation was carried out on an RP–C18 column HPLC ($250 \text{ mm} \times 4.6 \text{ mm}$, $5 \mu\text{m}$ particle size, Leonberg, Germany) with UV–Vis detector. The mobile phase consisted of ammonium acetate (0.05 M at pH 5.5), ACN in ratio of 55: 45, and v/v at a flow rate of 1 mL min^{-1} .

Synthesis of CDs

CDs have been synthesized by hydrothermal method. In brief, 0.5 g of dry powder of Valerian roots was mixed with 40 mL of distilled water and the mixture was placed in an autoclave and heated at $180 \text{ }^\circ\text{C}$ for 12 h. The bulky particles were removed from the consequential solution by centrifuging at 12,000 rpm for 20 min and filtration using a $0.45\text{-}\mu\text{m}$ filter membrane and centrifugal filters (10 kDa MW cutoff). The obtained CD solutions were kept at $4 \text{ }^\circ\text{C}$ in a dark place for further characterization and use.

Synthesis of MB

High surface area mesoporous boehmite (MB) of specific morphology was synthesized via a cost effective, green, and surfactant free method in a short time [17]. To obtain the

nanoboehmite, a solution of aluminum 2-propoxide in 2-propanol was hydrolyzed around the boiling point of 2-propanol by addition of acetic acid aqueous solution, followed by aging at reflux temperature for 24 h. The sample was then dried at 70 °C for 3 h at a pressure of 120 mbar.

Synthesis of CDs/MB

For the synthesis CDs/MB, a mixture of 4% mass ratio of CDs/MB was prepared. After stirring for 8 h, the doped materials were centrifuged (10,000 rpm/ 20 min). The residual precipitate was filtered and dried at room temperature [24]. The synthesis of CDs/MB was based on interaction between functional groups of CDs and MB. The CDs/MB was used for determination of different concentrations of IMI.

Quantum yield measurements

The quantum yield of CDs, which is generally dependent on the synthesis method employed, the nature of the precursors, and the passivation method used, was obtained through Eq. (1), Rhodamine-6G ($Q = 0.31$) being used as a standard sample.

$$Q_c = Q_r \cdot I_c / I_r \cdot A_r / A_c \cdot \eta_c^2 / \eta_r^2 \quad (1)$$

Here, Q denotes QY of CDs, A is the absorbance at the excitation wavelength, I is the integrated emission under fluorescence spectrum, η is the refractive index of the solvent, the subscript r and c indicate respectively the standard and sample [25].

Fluorescent assays

For the determination of IMI, a mixture of 40 μL (2.34 mg mL^{-1}) of CDs or 100 μL (1.00 $\mu\text{g mL}^{-1}$) of CDs/MB was mixed with the appropriate amount of the sample solutions and subtilized with universal buffer solution (pH = 6.0). When the excitation wavelength was 400 nm, the fluorescence intensity of the solution was recorded in the range of 420–700 nm. The excitation and emission slit widths used for recording the fluorescence spectra were 10.0 nm.

The response factor (F0-F) values were obtained and the sensitivity of the assay was evaluated. F0 and F correspond to the maximum fluorescence intensity in the absence and presence of IMI, respectively. The maximum fluorescence intensity was recorded at 485 and 483 nm excitation wavelengths in the presence of CDs and CDs/MB, respectively.

Study of cytotoxicity CDs

Given the numerous types and properties of CDs, they have a wide range of biomedical and biological applications.

The cytotoxicity of CDs has an important effect on cell growth and viability and has been observed in numerous in vitro studies. Some excellent properties of CDs have been discovered and applied in many areas of our lives. More and more people have an awareness of the benefits of CDs. However, the corresponding disadvantages still need to be considered.

Therefore, the cytotoxicity of the synthesized CDs was determined via an MTT assay. Two types of cancer cells, HeLa and HepG2, were plated separately in 96-well plates at 10,000 cells/well for 24 h. The cells were then exposed to the increasing concentration of CDs for 48 h at 37 °C. Thereafter, the cells were incubated for 3 h with 10 μL of MTT dye per well of the plate. Absorbance was measured at 490 nm and the results represent the mean values from three independent experiments [26].

Sample preparation

The blood plasma samples of several volunteers were obtained from the clinic center of the Isfahan University of Technology. The samples were diluted and filtered with syringe filters several times in order to separate any particles. The standard addition method was applied to different concentrations of IMI spiked to the serum.

For this evaluation, 350 μL of the filtered plasma sample was added to the solution containing 39.0 $\mu\text{g mL}^{-1}$ CDs, pH = 6.0. Afterwards, 400.0 μL of the serum sample was added into 2.6 mL of the mixture containing 1.00 $\mu\text{g mL}^{-1}$ of CDs/MB, pH = 6.0. After preparation, the fluorescence spectrum was recorded at 400 nm excitation wavelength in the range of 420–700 nm.

Cell viability assay

For studying the biocompatibility of green, synthesized CDs, the cell viability of the two types of cancer cells, HeLa and HepG2, were obtained using Eq. (2) [26]. The results showed that the cytotoxicity of the synthesized CDs was very low and more than 80% of these cells survived in the presence of CDs.

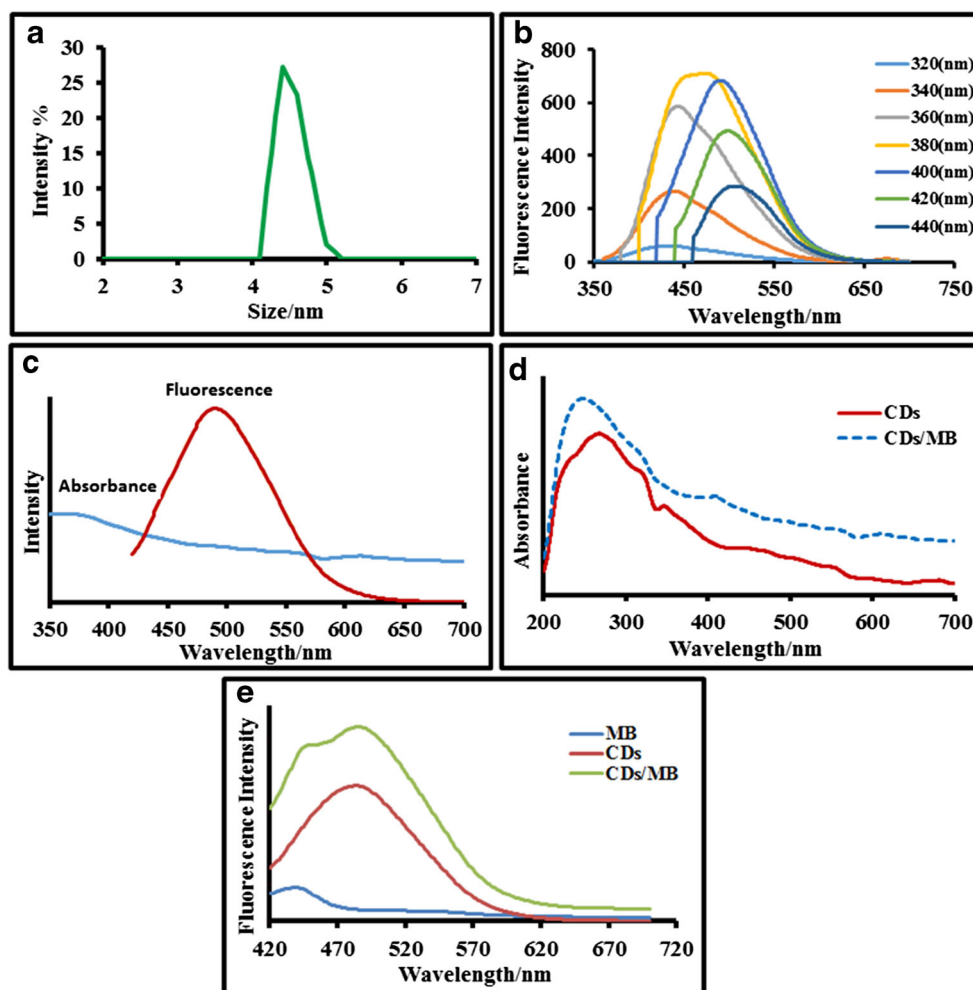
$$\text{Cell viability} = \frac{Abs_s}{Abs_c} \times 100 \quad (2)$$

Results and discussion

Characterization of the synthesized CDs

DLS technique was used to display the average diameter and size distribution of CDs. Fig. 1a shows that the synthesized CDs have a narrow distribution of 4.1–5.3 nm with the average size of 4.5 ± 0.4 .

Fig. 1 **a** DLS analysis of CDs; **b** the emission spectrums of CDs in different excitation wavelength; **c** absorbance and fluorescence emission of CDs; **d** comparison absorbance spectrums of CDs and CDs/MB; **e** comparison emission spectrums of CDs, MB, and CDs/MB



The absorbance and fluorescence emission spectra of CDs were recorded. Figure 1b shows the emission spectra of CDs at different excitation wavelengths. As it can be observed, the emission signal is higher at 400 nm excitation wavelength. Thus, 400 nm was selected as the excitation wavelength for analytical assays.

The emission wavelength of CDs relies heavily on the excitation wavelength, which is common to CDs produced [27].

Effective factors on the fluorescent behavior of the compounds included the nature of any substance, structure, and rigidity. As seen in previous works, MB with rigid structure was used to disperse the carbon nanoparticles and is mesoporous making it a good candidate to enhance fluorescence in solution. After dispersion of CDs on the MB, these CDs showed stronger photoluminescence with excellent stability against pH [28].

Characterization of CDs typically includes UV–visible absorption and fluorescence spectroscopy due to their optical properties [13]. The synthesized CDs show strong absorption in the UV–Vis region.

As it can be observed, the emission spectra of CDs are narrow and symmetrical, which makes it easy to distinguish one color of CD from another. Figure 1c shows the emission

spectra with a maximum at 485 nm under an excitation wavelength of 400 nm.

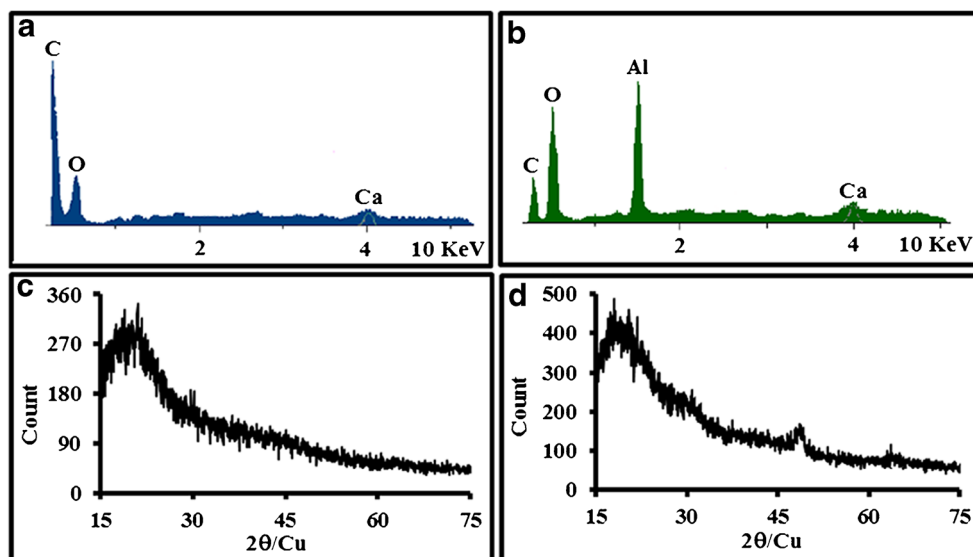
The absorbance spectra of CDs and CDs/MB are compared in Fig. 1d. Maximum absorbance wavelengths of CDs and CDs/MB were in 281 and 258 nm, respectively, and the absorbance intensity of CDs/MB was higher than that of CDs. Therefore, the fluorescence emission intensity of CDs/MB was greater than that of CDs.

As can be seen in (Fig. 1e), MB has the low intensity fluorescence in \sim 440 nm. That is different with the maximum wavelength fluorescence of CDs and was not interfered with quantitative measurements.

EDX patterns were studied to obtain the chemical composition of CDs and CDs/MB. As observed in Fig. 2a, major elements of CDs are carbon and oxygen. Furthermore, Fig. 2b shows oxygen, aluminum, and carbon in the CDs/MB.

XRD method was used to study the structure of CDs and CDs/MB (Fig. 2c and d). The XRD pattern of CDs/MB includes a band at 20° with an intensity greater than that of CDs. This peak emphasizes the amorphous structure of CDs/MB. Furthermore, two peaks are observed at 50° and 65° with low intensity, which are related to the crystalline structure of MB [17].

Fig. 2 a EDX pattern of CDs; b EDX pattern of CDs/MB; c XRD pattern of CDs; d XRD pattern of CDs/MB



TEM was used to study the shape and size of the synthesized CDs and CDs/MB. TEM images of synthesized CDs indicate CDs are made spherical and smaller than 10 nm in size (Fig. 3a).

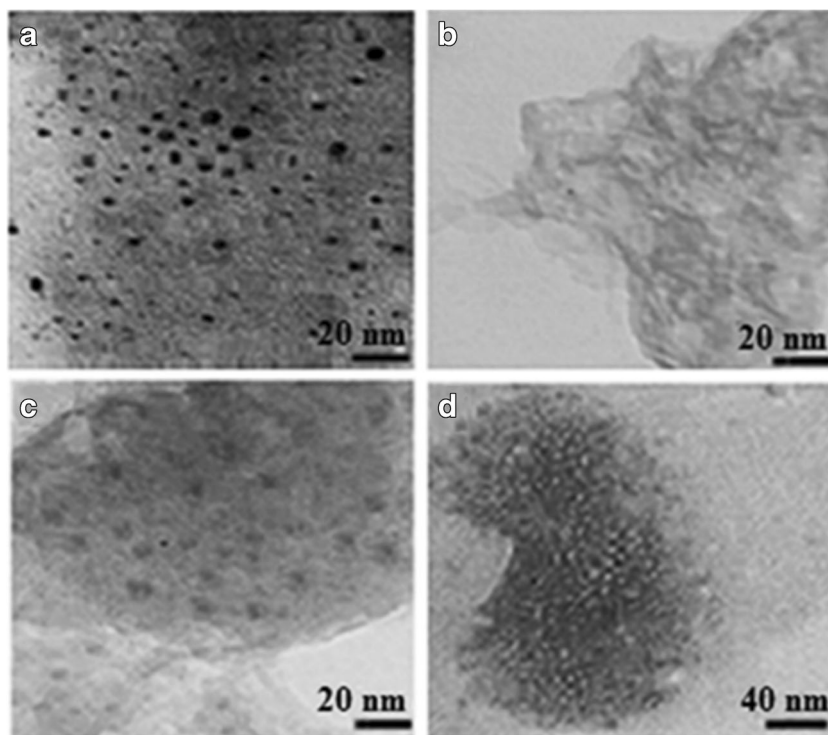
Moreover, the surface charge of CDs was negative at pH 6.0 and the zeta potential of CDs was negative (-18.5 ± 2.1 mV) as well. The electrostatic repulsion between CDs forms a stable colloidal condition.

At environmental conditions ($pK_a = 9.4$), IMI carry a positive charge in aqueous solution and the effective charge of the *N*-terminal amino group of IMI (z_{IMI}) is about +0.95 at pH = 7.4. Studies show pK_b of IMI at neutral pH is equal to 4.6 that

emphasize the amino structure of IMI [29]. Therefore, amino group in IMI becomes more positive at acidic pH. Zeta potential was measured. The zeta potential value for IMI was $+17.1 \pm 2.5$ mV that imparts a positive surface charge on the IMI.

Figure 3b shows the TEM images of MB, which indicate a well-defined structure layered. Moreover, this method can be used to estimate the surface size and shape and layer thickness. Figure 3c shows the morphology of CDs/MB. The CDs with spherical shape and size under 10 nm were dispersed in the layers of MB. The modified MB was formed due to hydrogen bonding between MB and CDs.

Fig. 3 a TEM images of CDs; b TEM images of MB; c TEM images of CDs/MB; d TEM images of CDs after addition of IMI



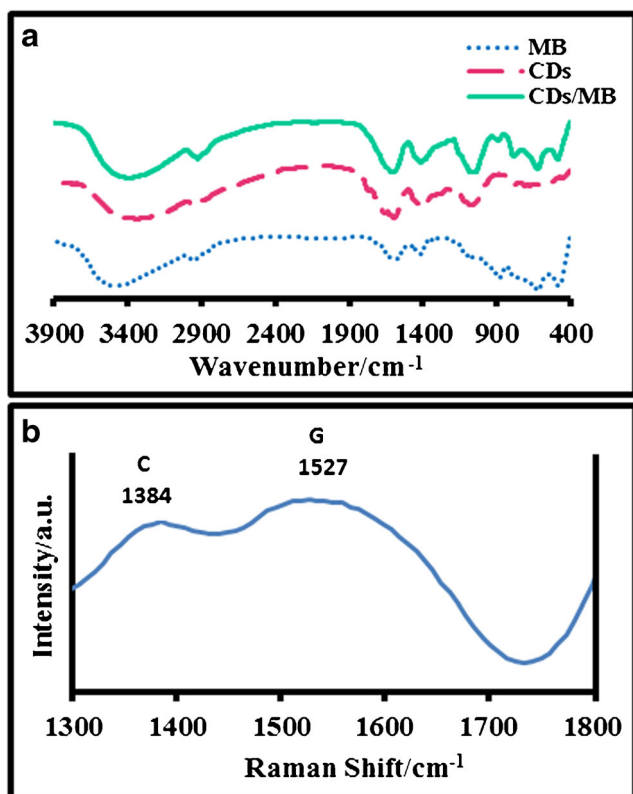


Fig. 4 a FTIR spectra of CDs and CDs/MB; b Raman spectra of CDs

The TEM analysis of CDs after the addition of IMI provides evidence for the aggregation of these nanoparticles

(Figure 3d). The aggregation of CDs by IMI occurs when smaller particles are deposited onto larger particles through an electrostatic interaction between negatively charged CDs with positively charged IMI.

Fourier-transform infrared (FTIR) spectroscopy has been extensively used to investigate the surface nature of nanoparticles [11]. Figure 4a shows the FTIR spectra of CDs and CDs/MB. Asymmetric and symmetric stretches of the carboxylate group are emerged at 1570 and 1391 cm⁻¹, respectively. In addition, the overlap of the -OH/-NH can be observed at 3200–3500 cm⁻¹ [30]. Other peaks show hydrocarbon groups on the CDs.

The template or content of the MB can be identified using FTIR. The FTIR spectra of synthesized CDs/MB also show two peaks at 621 and 868 cm⁻¹ related to the Al-OH and Al-O-Al, respectively [31]. The FTIR spectra of CDs/MB show both CDs and MB groups and the intensity peak of the hydroxyl group have not changed after MB modification [32].

Raman spectroscopy is a valuable technique for investigating the detailed bonding structure of the CDs. The Raman spectra of synthesized CDs show two peaks in 1385 and 1562 cm⁻¹ with different intensities corresponding to diamond (D) and graphite (G) bands, respectively (Fig. 4b). The ratio of the peak intensity of D-band to G-band (DI/GI) was 0.7, which confirms the graphitic structure of synthesized CDs [33, 34].

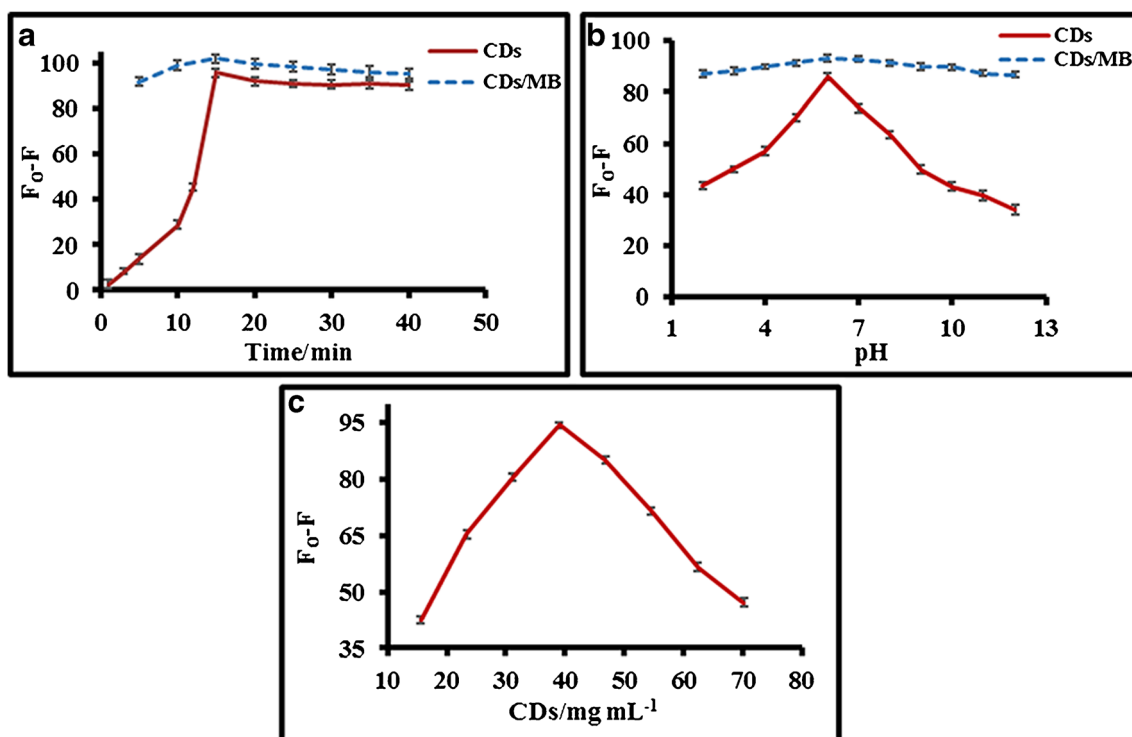


Fig. 5 a Effect of pH in determination IMI with CDs and CDs/MB as a fluorescence probe; b effect of concentration of CDs in determination IMI; c effect of time reaction in determination IMI with CDs and CDs/MB as a fluorescence probe

Optimization of reaction conditions

Effect of sample solution pH

Influences of different experimental variables on the response factor (F_0-F , where F_0 and F correspond to fluorescence intensity in the absence and presence of IMI) were studied. The effect of pH was examined over the range of 2–12 in the solution containing $39 \mu\text{g mL}^{-1}$ of CDs and 60 ng mL^{-1} of IMI. Figure 5a shows the carboxyl groups of CDs were protonated in an acidic pH. Therefore, the fluorescence signal of the probe was quenched due to its agglomeration [35]. The zeta potential of the synthesized CDs was negative at pH 6.0 and the fluorescence signal was maximum, which is the best value for determination of IMI. IMI is positively charged at pH 6.0 while this surface charge is hydrated at basic pH. An electrostatic interaction can occur between CDs and IMI at optimum pH, followed by the aggregation of CDs at pH 6.0. In addition, the pH in the presence of CDs/MB did not considerably influence the response factor of the probe. When MB was modified with CDs, the hydroxyl groups of the CDs were involved with those of MB and the pH of the solution did not affect the fluorescence emission intensity of the probe. The hydrogen bonding between CDs and MB can intercept the protonation and deprotonation of CDs in different pHs [36].

Effect of concentration CDs

The influence of different concentrations of CDs was studied on the response of the probe. When the concentration of IMI was 60.0 ng mL^{-1} and the pH of the universal buffer was 6.0, the response factors of different amounts of the CDs were measured (Fig. 5b). The results show the best response of the IMI probe was obtained in $39.0 \mu\text{g mL}^{-1}$ of CDs. At higher concentrations, the fluorescence signal was decreased due to the self-quenching of CDs. On the other hand, the signal to noise ratio was decreased if the concentration of CDs was too low [11, 35].

Effect of reaction time

The influence of different reaction times between CDs and IMI on the fluorescence intensity was studied. In a solution containing 60.0 ng mL^{-1} of IMI and $39.0 \mu\text{g mL}^{-1}$ of CDs at pH 6.0, the response factor (F_0-F) of different reaction times in the range of 1 to 40 min was recorded. The results show that 15 min is the best reaction time (Fig. 5c). This could be due to the completion of the reaction. Thus, 15 min was selected as optimum reaction time for further experiments.

The results of different reaction times between CDs/MB ($1 \mu\text{g mL}^{-1}$) and IMI (40.0 ng mL^{-1}) were obtained. As

observed in Fig. 5c, different reaction times have no considerable influence on the sensitivity of the CDs/MB probe because of completing the groups on the surface of CDs and thus the reaction time remains constant [36].

Given the more active surface area of MB, the reaction completed very fast and the effect of reaction time on the signal was not significant. The fast response can be illuminated by enhancing the electron transfer in the porous structure by the forward bias-induced barrier lowering [37].

Figure of merit

The fluorescence spectra of different concentrations of IMI ($1\text{--}200 \text{ ng mL}^{-1}$) under the optimum condition are shown in Fig. 6a. The response factor (fluorescence quenching of CDs) clearly depended on the concentration of IMI. It was shown that a linear relationship existed between (F_0-F) and $\log C$ (C is the concentration of IMI). In the linear range of $1.0\text{--}200.0 \text{ ng mL}^{-1}$, the correlation coefficient was 0.992. The theoretical limit of detection (LOD) was calculated by $3 S_b/m$, where m is the slope of the calibration diagram and S_b is the standard

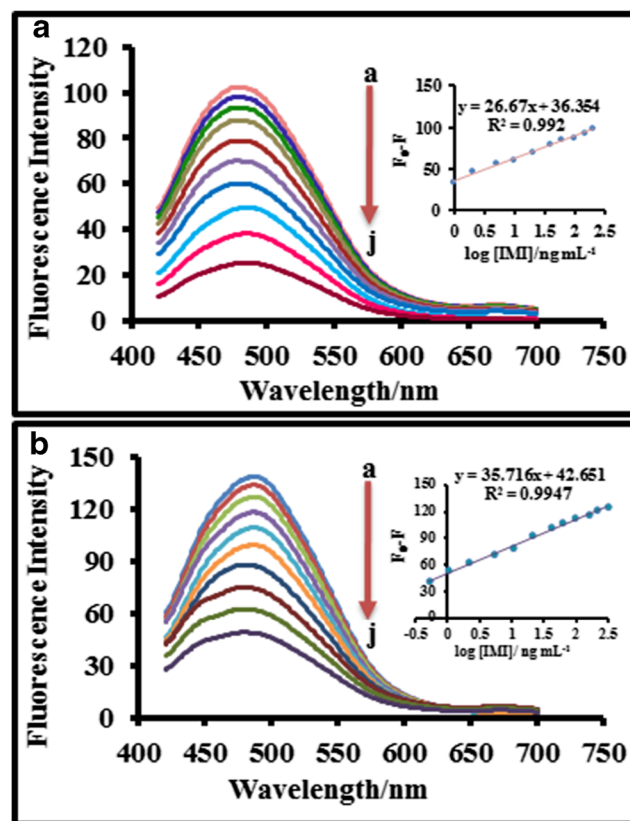


Fig. 6 Fluorescence spectra of calibration curve (a) $39.0 \mu\text{g mL}^{-1}$ CDs at pH = 6.0 in the presence of different concentrations of IMI as (a) 1 (b) 5 (c) 10 (d) 20 (e) 40 (f) 60 (g) 100 (h) 120 (i) 150 (j) 200 ng mL^{-1} . (b) $1.0 \mu\text{g mL}^{-1}$ CDs/MB and different concentration of IMI as (a) 1 (b) 2 (c) 3 (d) 5 (e) 10 (f) 20 (g) 40 (h) 60 (i) 90 (j) 120 (k) 150 (l) 200 ng mL^{-1}

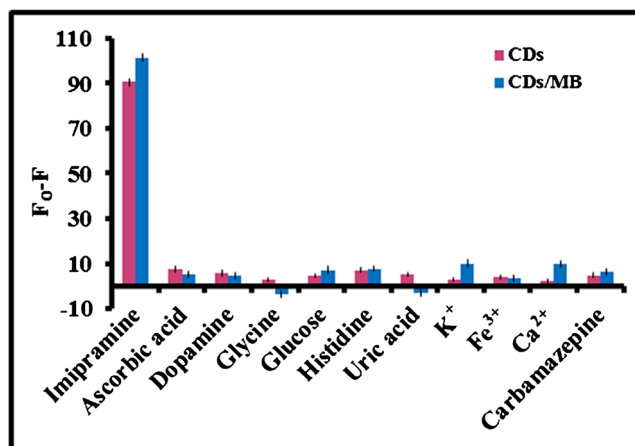


Fig. 7 Fluorescence response of CDs, $39.0 \mu\text{g mL}^{-1}$; IMI, 60 ng mL^{-1} and in the presence of different species interference, $60,000 \text{ ng mL}^{-1}$ and CDs/MB, $1 \mu\text{g mL}^{-1}$; IMI, 40 ng mL^{-1} and different species, $40,000 \text{ ng mL}^{-1}$

deviation of the blank ($n = 10$). The LOD was obtained at 0.6 ng mL^{-1} IMI. On the other hand, the experimental limit of detection was recorded as 1 ng mL^{-1} . The relative standard deviation (RSD) for a set of 5 measurements for 10.0 and 80.0 ng mL^{-1} IMI under the optimum conditions was obtained as 1.2 and 1.0% , respectively. In the fluorescence spectrum, the red-shift of maximum wavelengths is due to the decreased distance between CDs upon the addition of IMI [35]. Besides, Fig. 6b shows the fluorescence intensity of $1 \mu\text{g mL}^{-1}$ CDs/MB with different concentrations of IMI.

The correlation coefficient was obtained as 0.9947 in the liner range of $0.5\text{--}200.0 \mu\text{g mL}^{-1}$ of IMI. When CDs/MB was used as a probe, LOD was calculated at 0.2 ng mL^{-1} ($n = 10$) and RSD was 1.2 and 1.02% ($n = 5$) for 5 and 60 ng mL^{-1} , respectively. Considering the presence of carboxyl groups on the CDs, hydrogen bonding was formed between CDs and IMI, which probably increased the electron transfer rate from CDs to IMI and quenching mechanism occurred better [32].

Table 1 Determination IMI in real samples in the presence of CDs

Serum sample	IMI added (ng mL^{-1})	IMI found (ng mL^{-1})	RSD (%)	Recovery (%)
A	100.0	95.8	2.3	95.8
	150.0	146.5	1.7	97.7
B	50.0	55.8	2.7	111.5
	150.0	147	1.4	98
C	70.0	64.5	2.8	92.8
	100.0	107.9	1.2	107.9
	150.0	150.6	1.3	100.6

Table 2 Determination IMI in real samples in the presence of CDs/MB

Serum sample	IMI added (ng mL^{-1})	IMI found (ng mL^{-1})	RSD (%)	Recovery (%)
D	75.0	73.01	1.5	96.3
	100.0	100.9	1.3	100.7
	150.0	153	1.6	102.4
E	50.0	48.6	2.3	97.2
	150.0	153.6	1.6	102.4
F	50.0	54.2	2.0	108.4
	150.0	159.5	1.5	106.3

Interference

In order to study the effects of different species in the blood on the response of the assay based on CDs, the effect of ions such as Ca^{2+} , K^+ , Fe^{3+} , and organic compounds in the blood including ascorbic and uric acids, and several amino acids such as dopamine, histidine, glucose and glycine, and drug used with IMI, carbamazepine [38] were investigated. All of the interferences in $4500.0 \text{ ng mL}^{-1}$ and concentration of IMI was 60.0 ng mL^{-1} . A high concentration of interference was selected to ensure the interference effects.

The results in Fig. 7 indicate that the response of CDs to IMI was much more than that of interference species.

A strong interaction between CDs and IMI arising from the conflict surface charges can be the reason for the selectivity of this method. In the presence of CDs/MB, in the presence of $3000.0 \text{ ng mL}^{-1}$ of several spices and 40.0 ng mL^{-1} of IMI was studied. IMI was measured with high sensitivity and without noticeable interference effect due to the strong hydrogen bonds between CDs/MB and IMI (Fig. 7).

Applications

Application of CDs and CDs/MB as probes for determination of IMI in the serum samples was studied. IMI was measured in the real samples with the standard addition method. The results in Tables 1 and 2 show that the recovery percent of these probes in different serum samples is acceptable. The student t test was used to make sure the data accuracy in this method. The capability of these sensors for imipramine detection in real samples

Table 3 Determination IMI in urine samples

Sample	Proposed method ^a (ng mL^{-1})	HPLC ^a (ng mL^{-1})	t_{cal} ($t_{\text{table}}(95\%, 4) = 2.78$)
CDs	31.7 ± 1.2	36.9 ± 2.6	2.28
CDs/MB	33.2 ± 1.1	36.9 ± 2.6	1.65

^a Average values of three determinations \pm standard deviations

Table 4 Comparison results of some analytical methods for the determination IMI

Method	Reagent	Linear range (ng mL ⁻¹)	Detection limit (ng mL ⁻¹)	Ref.
Spectrophotometry	Chlordiazepoxide	9.81×10^2 – 2.0×10^4	2.85×10^2	[2]
	Fe (III) SCN–complex	2.53×10^2 – 3.16×10^2	2.53×10^2	[3]
RP-UPLC	UV detection/220 nm	1.9×10^2 – 2.97×10^3	0.25	[4]
HPLC-DLLME	UV detection	5.06 – 1.01×10^2	0.63	[5]
RP-HPLC/ ODS	UV detection/250 nm	2.0×10^3 – 1.2×10^4	–	[7]
Electrochemical	Ionic liquid electrode modified with montmorillonite nanoclay	31.6 – 6.33×10^2	6.33	[8]
electrochemiluminescence	Ru (byp) ₃ ²⁺	8.86 – 4.43×10^2	1.3	[9]
IMS	Composite of poly pyrrole and poly (ε-caprolactone)	44.3 – 2.34×10^2	0.63	[10]
Spectrofluorometry	CDs	1.0–200.0	0.6	This work
	Boehmite modified with CDs	0.5–200.0	0.2	This work

was examined by comparing the concentration of the imipramine in the urine sample of a patient using this drug.

The obtained results were compared with those achieved by HPLC method. After dispersive liquid–liquid microextraction of imipramine in human urine samples, HPLC-UV was used for the determination of the imipramine [39]. The *t* test results presented in Table 3 demonstrate the accuracy of the method.

Conclusion

In this work, simple, rapid, selective, and sensitive methods were developed for satisfactory determination of IMI by the fluorescent method based on green CDs and CDs/MB. The CDs were synthesized from Valerian root for the first time. When MB was modified with CDs, the fluorescence intensity increased and sensitivity in the determination of IMI improved.

After the addition of IMI, fluorescence quenching was observed, which was due to the reaction between CDs and IMI. The fluorescence quenching of the bare CDs with IMI was due to the aggregation of CDs. Electrostatic interaction between the negatively charged surfaces of CDs and positively charged IMI produced a significant reduction of the fluorescence signals.

The second interaction involves electron transfer between CDs on the MB and IMI. The protonated IMI may interact with the oxygenated surface of CDs located on the MB by hydrogen bonding, causing quenching of fluorescence.

The results of the employed method in this work showed a wide linear range and low limit of detection. The responses of the synthesized fluorescence probes were unaffected by different species in the body fluids, indicating the high selectivity of this method. To investigate the accuracy of this method, the results were compared with those of other reported methods such as spectrophotometry, UPLC, HPLC, electrochemical, IMS, electrochemiluminescence, and spectrofluorometry.

Table 4 shows the proposed method employing a simple green system with good sensitivity and selectivity.

Acknowledgments The authors wish to thank Research Council and Center of Excellence in Sensor and Green Chemistry of Isfahan University of Technology (IUT).

Compliance with ethical standards

Ethical approval All individual participants' blood plasma samples were obtained from the clinic center of the Isfahan University of Technology that were approved and supervised by the clinic center Committee. All experiments were performed in accordance with the ethical standards (Helsinki declaration and national, institutional rules and regulations).

Conflict of interest The authors declare that they have no conflict of interest.

References

- Marmot M. Social determinants of health inequalities. *Lancet*. 2005;365:1099–104.
- Patel SK, Patel NJ. Simultaneous determination of imipramine hydrochloride and chlordiazepoxide in pharmaceutical preparations by spectrophotometric, RP-HPLC, and HPTLC methods. *J AOAC Int*. 2010;93:904–10.
- Soni P, Sar SK, Kamavisdar A, Patel R. Simple and sensitive spectrophotometric method for determination of tricyclic antidepressant imipramine using Fe (III)-SCN- complex. *Anal Chem*. 2011;66:596–9.
- Deepakumari HN, Vinay KB, Revanasiddappa HD. Development and validation of a stability indicating RP-UPLC method for analysis of imipramine hydrochloride in pharmaceuticals. *Anal Chem*. 2013;2013:1–10.
- Shamsipur M, Mirmohammadi M. High performance liquid chromatographic determination of ultra traces of two tricyclic antidepressant drugs imipramine and trimipramine in urine samples after their dispersive liquid–liquid microextraction coupled with response surface optimization. *J Pharm Biomed Anal*. 2014;100:271–8.

6. Uguz F, Aydin A, Ak M, Turgut K. Low-dose imipramine for the treatment of panic disorder during postpartum period: a retrospective analysis of 6 cases. *J Clin Psychopharmacol.* 2016;36:292–3.
7. Srivastava V. Development and validation of RP-HPLC method for diazepam and imipramine in bulk & pharmaceutical formulations. *Pharmacophore.* 2016;7:63–73.
8. Eslami E, Farjam F. A sensitive electrochemical sensor for determination of imipramine in urine sample using carbon ionic liquid electrode modified with montmorillonite nanoclay. *Electrochemistry.* 2017;5:165–71.
9. Yu C, Du H, You T. Determination of imipramine and trimipramine by capillary electrophoresis with electrochemiluminescence detection. *Talanta.* 2011;83:1376–80.
10. Jafari M, Sedghi R, Ebrahimzadeh H. A platinum wire coated with a composite consisting of poly pyrrole and poly (ϵ -caprolactone) for solid phase microextraction of the antidepressant imipramine prior to its determination via ion mobility spectrometry. *Microchim Acta.* 2016;183:805–12.
11. Ensafi AA, Kazemifard N, Rezaei B. A simple and rapid label-free fluorimetric biosensor for protamine detection based on glutathione-capped CdTe quantum dots aggregation. *Biosens Bioelectron.* 2015;71:243–8.
12. Zheng XT, Ananthanarayanan A, Luo KQ, Chen P. Glowing graphene quantum dots and carbon dots: properties, syntheses, and biological applications. *Small.* 2015;11:1620–36.
13. Shahshahanipour M, Rezaei B, Ensafi Ali A, Etemadifar Z. An ancient plant for the synthesis of a novel carbon dot and its applications as an antibacterial agent and probe for sensing of anticancer drug. *Mater Sci Eng C.* 2019;98:826–33.
14. Cui X, Zhu L, Wu J, Hou Y, Wang P, Wang Z, et al. A fluorescent biosensor based on carbon dots-labeled oligodeoxyribonucleotide and graphene oxide for mercury (II) detection. *Biosens Bioelectron.* 2015;63:506–12.
15. Fernández-San-Martín MI, Masa-Font R, Palacios-Soler L, Sancho-Gómez P, Calbó-Caldentey C, Flores-Mateo G. Effectiveness of Valerian on insomnia: a meta-analysis of randomized placebo-controlled trials. *Sleep Med.* 2010;11:505–11.
16. Kamrani S, Rezaei M, Kord M, Baalousha M. Transport and retention of carbon dots (CDs) in saturated and unsaturated porous media: role of ionic strength, pH, and collector grain size. *Water Res.* 2018;133:338–47.
17. Khaleel A, Nawaz M. Enhanced catalytic complete oxidation of 1, 2-dichloroethane over mesoporous transition metal-doped γ -Al₂O₃. *J Environ Sci.* 2015;29:199–209.
18. Mohammadnezhad G, Akintola O, Plass W, Steiniger F, Westermann M. A facile, green and efficient surfactant-free method for synthesis of aluminum nanooxides with an extraordinary high surface area. *Dalton Trans.* 2016;45:6329–33.
19. Santos P de S, Coelho ACV, Santos H de S, Kiyohara PK. Hydrothermal synthesis of well-crystallised boehmite crystals of various shapes. *Mater Res.* 2009;12:437–45.
20. Raybaud P, Digne M, Iftimie R, Wellens W, Euzen P, Toulhoat H. Morphology and surface properties of boehmite (γ -AlOOH): a density functional theory study. *J Catal.* 2011;201:236–46.
21. Hajjami M, Ghorbani-Choghamarani A, Ghafouri-Nejad R, Tahmasbi B. Efficient preparation of boehmite silica dopamine sulfamic acid as a novel nanostructured compound and its application as a catalyst in some organic reactions. *New J Chem.* 2016;40:3066–74.
22. Aryal BP, Benson DE. Electron donor solvent effects provide biosensing with quantum dots. *J Am Chem Soc.* 2006;128:15986–7.
23. Adkins H, Cox FW. Relative oxidation-reduction reactivities of ketones and aldehydes and applications in synthesis I. *J Am Chem Soc.* 1938;60:1151–9.
24. Costas-Mora I, Romero V, Pena-Pereira F, Lavilla I, Bendicho C. Quantum dots confined in an organic drop as luminescent probes for detection of selenium by microfluorospectrometry after hydridation: study of the quenching mechanism and analytical performance. *Anal Chem.* 2012;84:4452–9.
25. Skoog DA, Holler FJ, Crouch SR. Principles of instrumental analysis. 6rd ed. Belmont: Thomson Brooks/Cole; 2007.
26. Matai I, Sachdev A, Gopinath P. Self-assembled hybrids of fluorescent carbon dots and PAMAM dendrimers for epirubicin delivery and intracellular imaging. *ACS Appl Mater Interfaces.* 2015;7:11423–35.
27. Kumari A, Kumar A, Sahu SK, Kumar S. Synthesis of green fluorescent carbon quantum dots using waste polyolefins residue for Cu²⁺ ion sensing and live cell imaging. *Sensors Actuators B Chem.* 2018;254:197–205.
28. Hariharan PS, Anthony SP. Selective fluorescence sensing of Mg²⁺ ions by Schiff base chemosensor: effect of diamine structural rigidity and solvent. *RSC Adv.* 2014;4:41565–71.
29. Jiang C, Wu H, Song X, Ma X, Wang J, Tan M. Presence of photoluminescent carbon dots in Nescafe® original instant coffee: applications to bioimaging. *Talanta.* 2014;127:68–74.
30. Sachdev A, Gopinath P. Green synthesis of multifunctional carbon dots from coriander leaves and their potential application as antioxidants, sensors and bioimaging agents. *Analyst.* 2015;140:4260–9.
31. Mohammadnezhad G, Dinari M, Nabiyan A. High surface area nano-boehmite as effective nano-filler for preparation of boehmite-polyamide-6 nanocomposites. *Polym Adv Technol.* 2016. <https://doi.org/10.1002/adv.21783>.
32. He Y, He J, Zhang H, Liu Y, Lei B. Luminescent properties and energy transfer of luminescent carbon dots assembled mesoporous Al₂O₃: Eu³⁺ co-doped materials for temperature sensing. *J Colloid Interface Sci.* 2017;496:8–15.
33. Ding H, Zhang P, Wang T-Y, Kong J-L, Xiong H-M. Nitrogen-doped carbon dots derived from polyvinyl pyrrolidone and their multicolor cell imaging. *Nanotechnology.* 2014. <https://doi.org/10.1088/0957-4484/25/20/205604>.
34. Atchudan R, Perumal S, Karthikeyan D, Pandurangan A, Lee YR. Synthesis and characterization of graphitic mesoporous carbon using metal-metal oxide by chemical vapor deposition method. *Microporous Mesoporous Mater.* 2015;215:123–32.
35. Rezaei B, Shahshahanipour M, Ensafi AA. A simple and sensitive label-free fluorescence sensing of heparin based on CdTe quantum dots. *J Lumin.* 2016;31:958–64.
36. Li S, Zhou S, Xu H, Xiao L, Wang Y, Shen H, et al. Luminescent properties and sensing performance of a carbon quantum dot encapsulated mesoporous silica/polyacrylonitrile electrospun nanofibrous membrane. *J Mater Sci.* 2016;51:6801–11.
37. Liu C-Y, Chen C-F, Leu J-P, Lu C-C, Liao K-H. Fabrication and carbon monoxide sensing characteristics of mesostructured carbon gas sensors. *Sensors Actuators B Chem.* 2009;143:12–6.
38. Szymura-Oleksiak J, Wyska E, Wasieczko A. Pharmacokinetic interaction between imipramine and carbamazepine in patients with major depression. *Psychopharmacology.* 2001;154:38–42.
39. Mohebbi A, Farajzadeh MA, Yariyapour S, Mogaddam MRA. Determination of tricyclic antidepressants in human urine samples by the three-step sample pretreatment followed by HPLC-UV analysis: an efficient analytical method for further pharmacokinetic and forensic studies. *EXCLI J.* 2018;17:952–63.

Publisher's Note Springer Nature remains neutral with regard to jurisdictional claims in published maps and institutional affiliations.